JCI insight

RESEARCH ARTICLE

SREBP-regulated adipocyte lipogenesis is dependent on substrate availability and redox modulation of mTORC1

Clair Crewe,[1] Yi Zhu,[1] Vivian A. Paschoal,[1] Nolwenn Joffin,[1] Alexandra L. Ghaben,[1] Ruth Gordillo,[1] Da Young Oh,[1] Guosheng Liang,[2] Jay D. Horton,[2,3] and Philipp E. Scherer[1]

[1]Touchstone Diabetes Center, [2]Department of Molecular Genetics, and [3]Center for Human Nutrition, University of Texas Southwestern Medical Center, Dallas, Texas, USA.

The synthesis of lipid and sterol species through de novo lipogenesis (DNL) is regulated by 2 functionally overlapping but distinct transcription factors: the SREBPs and carbohydrate response element–binding protein (ChREBP). ChREBP is considered to be the dominant regulator of DNL in adipose tissue (AT); however, the SREBPs are highly expressed and robustly regulated in adipocytes, suggesting that the model of AT DNL may be incomplete. Here, we describe what we believe to be a new mouse model of inducible, adipocyte-specific overexpression of the insulin-induced gene 1 (Insig1), a negative regulator of SREBP transcriptional activity. Contrary to convention, Insig1 overexpression did block AT lipogenic gene expression. However, this was immediately met with a compensatory mechanism triggered by redox activation of mTORC1 to restore SREBP1 DNL gene expression. Thus, we demonstrate that SREBP1 activity sustains adipocyte lipogenesis, a conclusion that has been elusive due to the constitutive nature of current mouse models.

Introduction

Cellular lipid synthesis is essential for organismal metabolic homeostasis, yet it can also be destructive if left unrestrained. For this reason, lipid production is tightly regulated. Lipid is generated through the process of de novo lipogenesis (DNL), whereby acetyl-coA derived from the mitochondrial oxidation of carbohydrates is converted into fatty acids or cholesterol species. Adipose tissue (AT) and liver are major lipogenic organs, coordinating the conversion of dietary sugars into fatty acids and subsequent storage in AT as triglycerides (TGs). DNL in AT is not considered a significant source of circulating lipids, compared with the liver, but it is essential to whole-body homeostasis due its pertinent role in storing potentially toxic excess sugars as chemically stable lipids (1). In obese mice and humans, AT lipogenic enzyme expression is reduced, leading to suppression of DNL flux (2–6). It is widely accepted that insulin resistance is positively correlated to DNL in the liver and negatively correlated to DNL in AT (3, 7, 8).

Two pathways coordinate the regulation of lipid biosynthesis genes: the SREBPs and carbohydrate response element–binding protein (ChREBP) (9, 10). The SREBP family of basic helix-loop-helix transcription factors consists of SREBP1a, SREBP1c, and SREBP2, which promote fatty acid production (SREBP1a/c) and cholesterol synthesis (SREBP2). SREBP proteins are synthesized as a membrane-bound, inactive form sequestered in the ER by association with Scap. The Scap protein senses an increase in cellular sterol concentration and maintains retention of the SREBPs in the ER through interaction with the insulin-induced gene 1 or 2 (Insig1 or Insig2). When sterol levels decline, such as in the postprandial state, conformational changes in Scap result in its dissociation from Insig1, freeing Scap to escort the SREBPs to the Golgi. Here, the SREBPs are cleaved into an active form and transported to the nucleus to stimulate the transcription of lipogenesis genes. In addition to sterol regulation of protein processing, SREBP1c mRNA is strongly induced by insulin through LXR transcriptional activation (11, 12). Downstream of insulin-stimulated AKT activation, the mechanistic target of rapamycin complex 1 (mTORC1) is a key positive regulator of SREBP1 mRNA transcription and SREBP1 processing (13).

DNL capacity is acutely regulated by availability of glucose and fructose; both of which serve as lipogenic substrates. This occurs through the activation of the ChREBP transcription factor by glycolytic intermediates,

Conflict of interest: The authors have declared that no conflict of interest exists.

Submitted: April 8, 2019
Accepted: July 9, 2019
Published: August 8, 2019.

Reference information: *JCI Insight*. 2019;4(15):e129397. https://doi.org/10.1172/jci.insight.129397.

such as xylulose 5-phosphate and glucose-6-phosphate. ChREBP induces the transcription of genes in both the DNL and glycolytic pathways (14, 15). Therefore, the presence of both insulin and lipogenic precursors generates a synergistic response through the actions of these two overlapping, yet distinct, lipogenic transcriptional pathways (14).

Regulation of DNL in AT is considered to be the exclusive responsibility of the ChREBP pathway, as ChREBP-KO mice exhibit complete repression of glucose- and fructose-stimulated lipogenesis in AT (15). In contrast, SREBP1-null mice do not display a reduction in AT lipogenic gene expression (8, 16). However, SREBP proteins are highly expressed in AT tissue and are greatly affected by refeeding, similar to their regulation in the liver (17). This implies that the SREBPs may participate in AT DNL, yet current experimental models have not detected a significant role for SREBPs to support this notion. To date, mouse models used to genetically suppress lipogenesis have either been whole-body KOs of essential lipogenic regulators or adipocyte-specific KOs using a constitutively expressed Cre-recombinase. These models have been pivotal for our current understanding of lipogenesis in AT; however, by nature, constitutive models are prone to developmental compensation. Here, we use a mouse model of inducible, adipocyte-specific Insig1 overexpression as a tool to study the effect of acutely obstructing SREBP-mediated lipogenesis in adult AT. Others have demonstrated that overexpression of Insig1 at high levels in cultured epithelial-like cells or in vivo hepatocytes can trap the SCAP/SREBP complex in the ER, independent of sterol concentrations, thereby precluding lipogenic gene expression (18, 19). Therefore, Insig1 overexpression can mimic the natural inhibition of DNL. We found that, within 12 hours of Insig1 induction, lipogenic enzyme levels were significantly reduced, followed by a striking *increase* in the same proteins at 24 hours and finally a return of these enzymes to control levels within 3 days. Initial inhibition of lipogenesis by Insig1 overexpression results in mitochondrial dysfunction, likely due to excess carbons entering oxidative phosphorylation, which would otherwise be shunted via the citrate transporter into the lipogenic pathway. The ensuing mitochondrially generated ROS results in mTORC1 activation and, thus, restoration of DNL enzyme expression. mTORC1 activation is transient, resolving within 3 days of Insig1 overexpression, but chronic compensation was facilitated by upregulation of the fructose transporter GLUT5. We demonstrate that chronic compensation does not occur in the absence of DNL substrates. Thus, similarly to ChREBP, the SREBP proteins are also regulated by substrate availability in AT through this mitochondria-mediated mTORC1 activation. In fact, our data suggest that this mechanism ensures that there is never a brake in AT lipogenesis in the presence of substrate. Furthermore, an important lesson from the current work is that, if essential pathways are genetically modified, rapid compensation may take effect through partially redundant pathways, necessitating a detailed analysis of the system during the immediate aftermath of the genetic intervention.

Results

Inducible, tissue-specific overexpression of Insig1 was accomplished through the generation of a transgenic mouse carrying the Insig1 gene driven by the tetracycline response element (TRE). This mouse was bred to another mouse that carried the reverse tetracycline transactivator (rtTA) under the control of the adiponectin promoter to restrict transgene expression to adipocytes (Figure 1A). Mice were provided with a diet containing doxycycline (dox) to induce Insig1 gene expression (Figure 1A). The resulting overexpression model is referred to as ad-Insig1. Insig1 is successfully overexpressed in AT but not in the liver, and expression is strictly dependent on dox (Figure 1B). Furthermore, Insig1 protein expression is successfully increased in subcutaneous AT (sWAT) 24 hours and 2 weeks after dox administration (Figure 1C). For the initial experiments, control and ad-Insig1 mice were maintained on high-fat diet containing dox for 16 weeks. Body weight, oral glucose tolerance, and TG clearance measurements were unaltered by adipocyte overexpression of Insig1 (Figure 1, D–F). We found that, although Insig1 mRNA remained highly expressed in sWAT after 16 weeks HFD, lipogenic genes were not suppressed as would be expected (Supplemental Figure 1A; supplemental material available online with this article; https://doi.org/10.1172/jci.insight.129397DS1). Scd1 mRNA is the exception, being reduced by 60% compared with control tissue (Supplemental Figure 1A). We hypothesized that the perceived lack of Insig1 function is the result of a compensatory mechanism that restores lipogenic gene expression. Thus, we took advantage of our inducible expression system and harvested AT at 12 hours following dox injection or after 3 days to 3 weeks of dox chow feeding. We observed an overall reduction in lipogenic genes at the 12-hour time point (Figure 1G), an effect that was reversed at 1 day when DNL genes were unchanged (Supplemental Figure 1B) and at 3 days when DNL genes trended

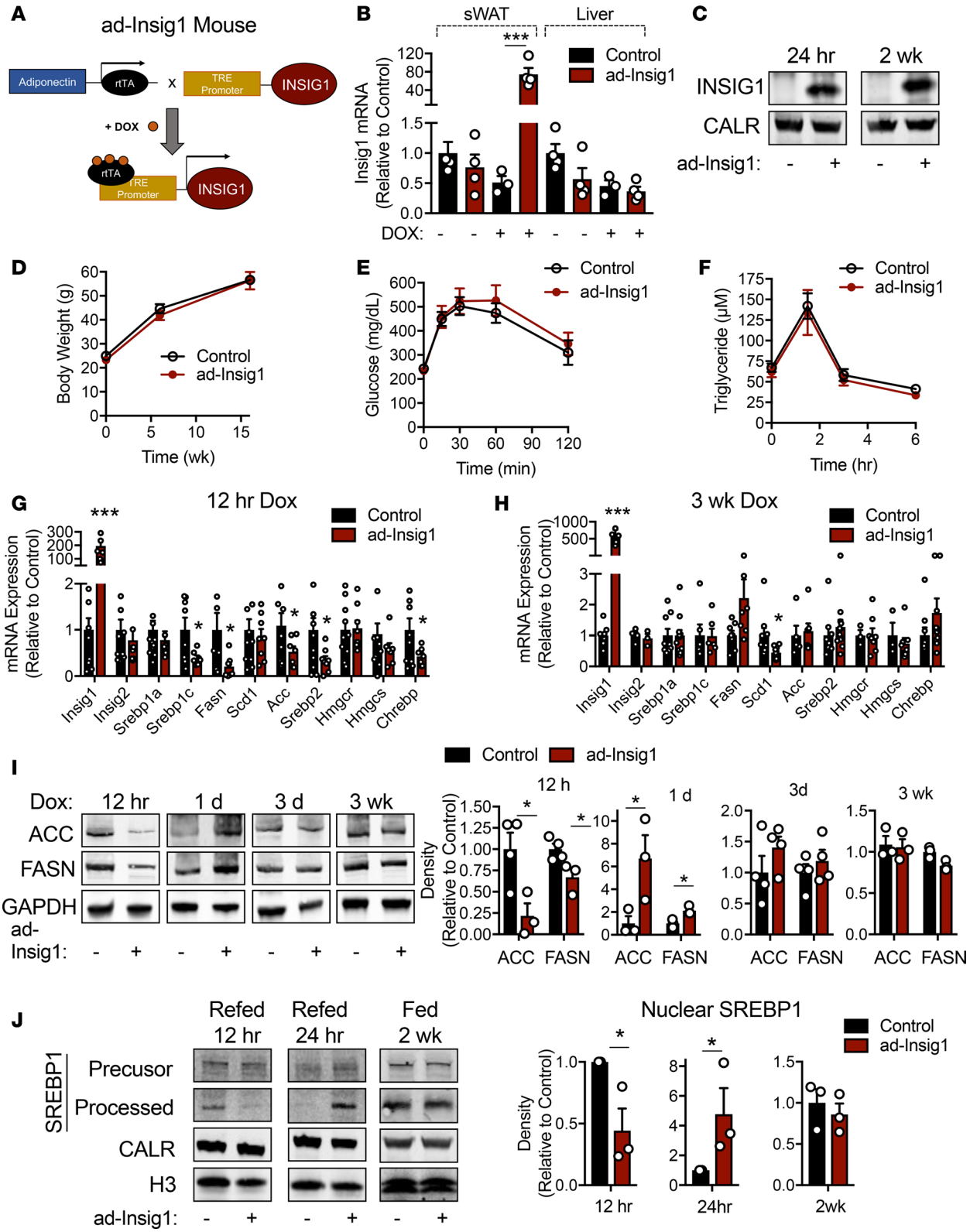

Figure 1. Overexpression of Insig1 in adipocytes results in suppression of lipogenesis followed by compensation. (**A**) Mouse model of inducible, adipocyte-specific overexpression of Insig1 (ad-Insig1). Doxycycline (dox) binds the reverse tetracycline transactivator (rtTA) expressed in adipocytes via the adiponectin promoter. The rtTA is thereby activated to bind the tetracycline response element (TRE) to drive Insig1 expression. (**B**) qPCR analysis of *Insig1* in sWAT or liver tissue from control and ad-Insig1 mice with or without dox treatment for 5 days (n = 3–4). (**C**) Insig1 protein expression in the ER membrane fraction of control or ad-Insig1 mouse sWAT treated with dox for 24 hours or 2 weeks. (**D**–**F**) Control or ad-Insig1 mice were provided a high-fat diet (HFD) containing dox for 16 weeks, during which (**D**) body weight was measured (n = 7). (**E**) An oral glucose tolerance test was conducted at 16 weeks on diet (n = 7), and (**F**) a triglyceride clearance test was performed at the 10-week time point on the same diet (n = 8). (**G**) Lipogenic gene expression in sWAT

12 hours after injection of 2 mg/kg dox (n = 8) or (**H**) 3 weeks of dox-containing chow diet (n = 5–8). (**I**) Representative Western blots and densitometry of ACC and FASN in sWAT at the indicated times of dox exposure (n = 3–4). Only the gel lanes that are cropped together can be compared. Blots for GAPDH were run separately from ACC and FASN, although consistent biological samples are presented. (**J**) Control and ad-Insig1 mice were fasted for 16 hours and refed dox-containing chow for 12 hours, 24 hours, or 2 weeks. sWAT tissue was separated into nuclear- and ER membrane–enriched fractions for processed and precursor SREBP1, respectively. Calreticulin (CALR) was used as a loading control from membrane fractions and histone 3 (H3) was used as the loading control for the nuclear fractions. Shown is a representative of n = 3 Western blots and corresponding densitometry of nuclear-located SREBP1. All data are presented as mean ± SEM. $^{*}P < 0.05$, $^{***}P < 0.001$ by 2-tailed Student's t test. In all cases, for a given condition, representative Western blot images are from the same sample, although the target proteins may have been probed on separate membranes to facilitate clear visualization. All densitometry was conducted on samples run on the same gel.

toward an increase (Supplemental Figure 1C). The suppression of DNL gene expression was completely lost at 3 weeks (Figure 1H). Again, the exception was SCD1 mRNA, which remained suppressed (Figure 1H). Interestingly, this compensation observed at 3 days did not occur in brown AT (Supplemental Figure 1D). At the protein level, 2 rate-limiting enzymes in DNL, ACC, and FASN were decreased in sWAT after 12 hours of dox treatment but significantly *increased* following 1 day of dox feeding and finally normalized to control levels at the 3-day and 3-week time points (Figure 1I). Similarly, fasted ad-Insig1 mice refed with dox-containing diet for 12 hours displayed less nuclear/processed SREBP1 in sWAT compared with control mice (Figure 1J). In contrast, if the refeeding period was extended to 1 day, ad-Insig1 mouse sWAT contained much higher levels of nuclear SREBP1 (Figure 1J). Furthermore, dox administration for 2 weeks resulted in normalization of SREBP1 levels (Figure 1J). sWAT ChREBP protein content trended toward an increase at 1 day of dox feeding; however, expression levels were highly variable in ad-Insig1 mice (Supplemental Figure 2). At 2 weeks of dox feeding, ChREBP levels were slightly decreased (Supplemental Figure 2), suggesting that ChREBP may not be a robust mediator of lipogenic gene restitution in ad-Insig1 mice. Taken together, these data validate that Insig1 overexpression indeed suppresses SREBP1-mediated lipogenesis in white AT; however, this block in lipogenesis is promptly reversed by some compensatory mechanism.

We went on to determine if the transient shifts in AT lipogenesis promoted by Insig1 overexpression are sufficient to alter whole-body metabolism. Three time points were chosen for basic phenotyping, with the caveat that these are snapshots in time while the AT is undergoing dramatic changes in signaling. Twelve hours after dox injection, a time point at which AT lipogenesis is reduced, ad-Insig1 mice displayed a slight impairment in an oral glucose tolerance test (Figure 2A) and a significant improvement in TG clearance (Figure 2B). The sWAT fat pad weight was increased and the visceral epididymal fat pad (eWAT) weight was not changed in ad-Insig1 mice at the 12-hour time point (Figure 2C). Although this result is unexpected for AT with reduced lipogenesis, it is likely that a longer period of DNL blockade is required to detect the expected decrease in fat pad weight. Additionally, no change in total body weight was observed (Figure 2D). After 3 days of dox feeding, AT lipogenesis was in the process of compensating (Figure 1I and Supplemental Figure 1C). At this time point, ad-Insig1 mice trended toward improved oral glucose tolerance (Figure 2E), and improvements observed in TG clearance at 12 hours were reversed at 3 days (Figure 2F). Furthermore, ad-Insig1 sWAT and eWAT mass were reduced (Figure 2G) without a change in body weight (Figure 2H) at 3 days. Reductions in fat pad mass can be attributed to both Insig1-mediated inhibition of lipogenesis as well as enhanced lipolysis, cellular processes that are known to be reciprocally regulated. After 3 days of dox feeding, ad-Insig1 mice exhibited a lipolytic phenotype, as evidenced by higher levels of unstimulated hormone sensitive lipase phosphorylation in sWAT (Supplemental Figure 3, A and B), increased glycerol release during an ex vivo lipolysis assay (Supplemental Figure 3C), increased lipase and fatty acid transporter mRNA expression (Supplemental Figure 3D), and slightly smaller adipocytes (Supplemental Figure 3E). After 3 weeks of dox feeding, when the AT had completely restored the ability to do DNL, glucose tolerance, TG clearance, fat pad weight, and body weight were not different between control and ad-Insig1 mice (Figure 2, I–L). Mouse models of liver DNL deficiencies have presented with compensatory enhancements in AT lipogenesis (20). Here, we found that such a level of interorgan compensation does not hold true for impairments in AT DNL, i.e., the lack of a phenotype at 3 weeks of dox feeding was not the result of enhanced liver lipogenesis (Figure 2M). These data suggest that changes in SREBP1-mediated DNL in AT would have a functional consequence for whole-body metabolic homeostasis if it was not for the self-correcting normalization of DNL at the level of AT itself.

Insulin is a major regulator of lipogenesis in AT and liver through the PI3-kinase/AKT-mediated mTORC1 pathway (21). mTORC1 is required for AKT-stimulated SREBP1 expression and processing (22). Blockade of mTORC1 activity results in loss of lipogenic gene expression (21–24). We determined

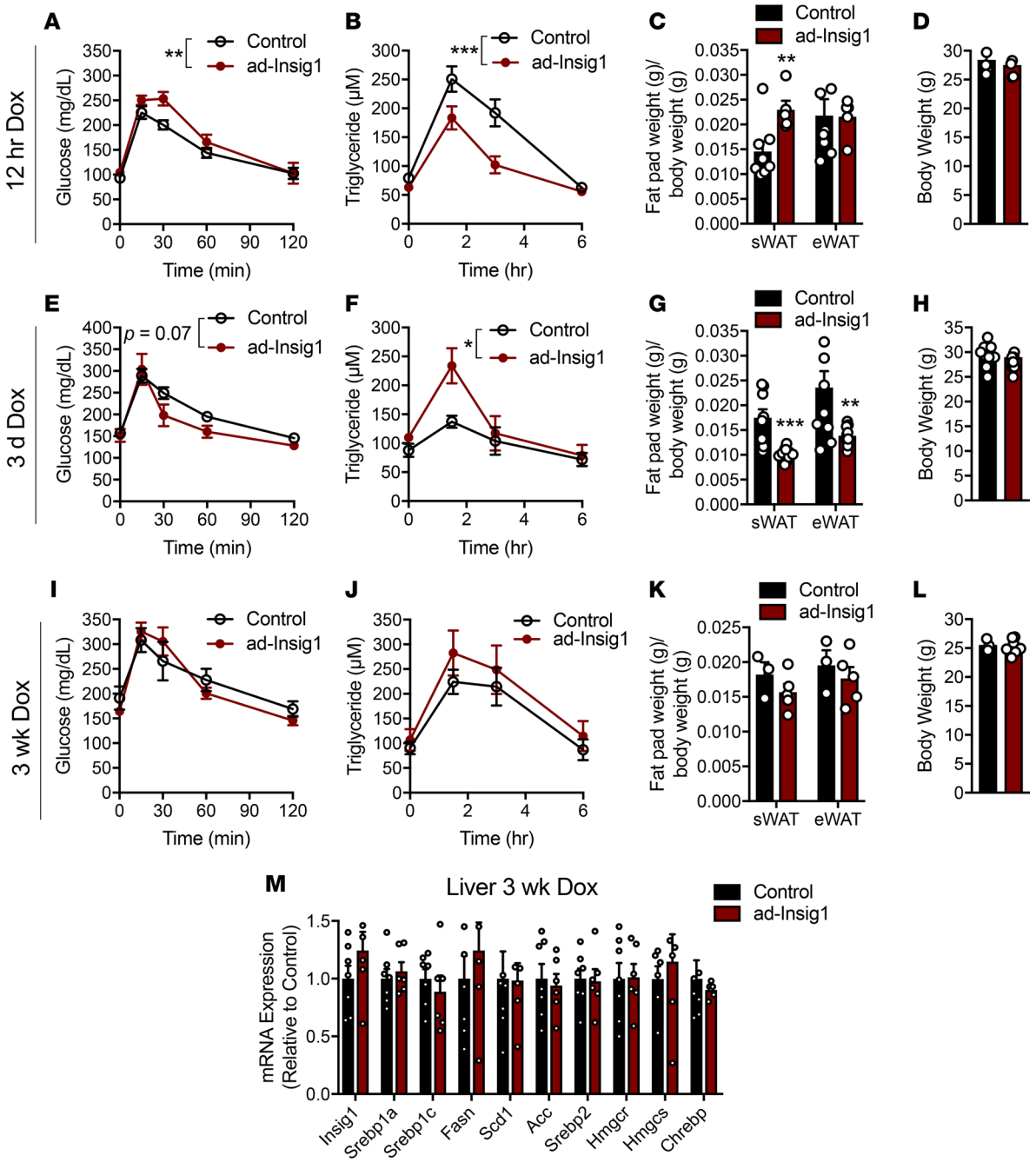

Figure 2. Manipulation of adipose DNL alters whole-body metabolism. (**A**–**D**) Twelve hours after dox injection (2 mg/kg) mice were subjected to an (**A**) oral glucose tolerance test (n = 6) and a (**B**) triglyceride clearance test (n = 9–10). At this 12-hour time point, another cohort of mice were used for (**C**) sWAT and eWAT depot weights (n = 8) and (**D**) total body weight (n = 8). (**E**–**L**) Mice were provided with chow diet containing dox for 3 days or 3 weeks, at which time mice were subjected to an (**E** and **I**) oral glucose tolerance test (n = 5–8) and a (**F** and **J**) triglyceride clearance test (n = 5–8) or (**G** and **K**) sacrificed for white AT weights. (**H** and **L**) Body weight measurements at the indicated times. (**M**) qPCR for lipogenic genes in liver of control and ad-Insig1 mice following 3 weeks of chow diet supplemented with dox (n = 7). All data are presented as mean ± SEM. *P < 0.05, **P < 0.01, ***P < 0.001 by 2-tailed Student's t test (bar graphs) or 2-way ANOVA (systemic assays).

whether mTORC1 participates in the observed compensatory mechanism. At 12 hours after dox injection, ad-Insig1 mice displayed a striking increase in phosphorylation of S6 ribosomal protein, which is a surrogate readout for mTORC1 activity (Figure 3, A and B). Phospho-S6 remained significantly elevated in ad-Insig1 mice compared with controls for a full 24 hours of dox feeding, before returned to control levels by 3 days (Figure 3B), a time-course similar to that observed for the reestablishment of lipogenic enzyme expression (Figure 1I). mTORC1 activation did not correlate with AKT activity, as basal levels

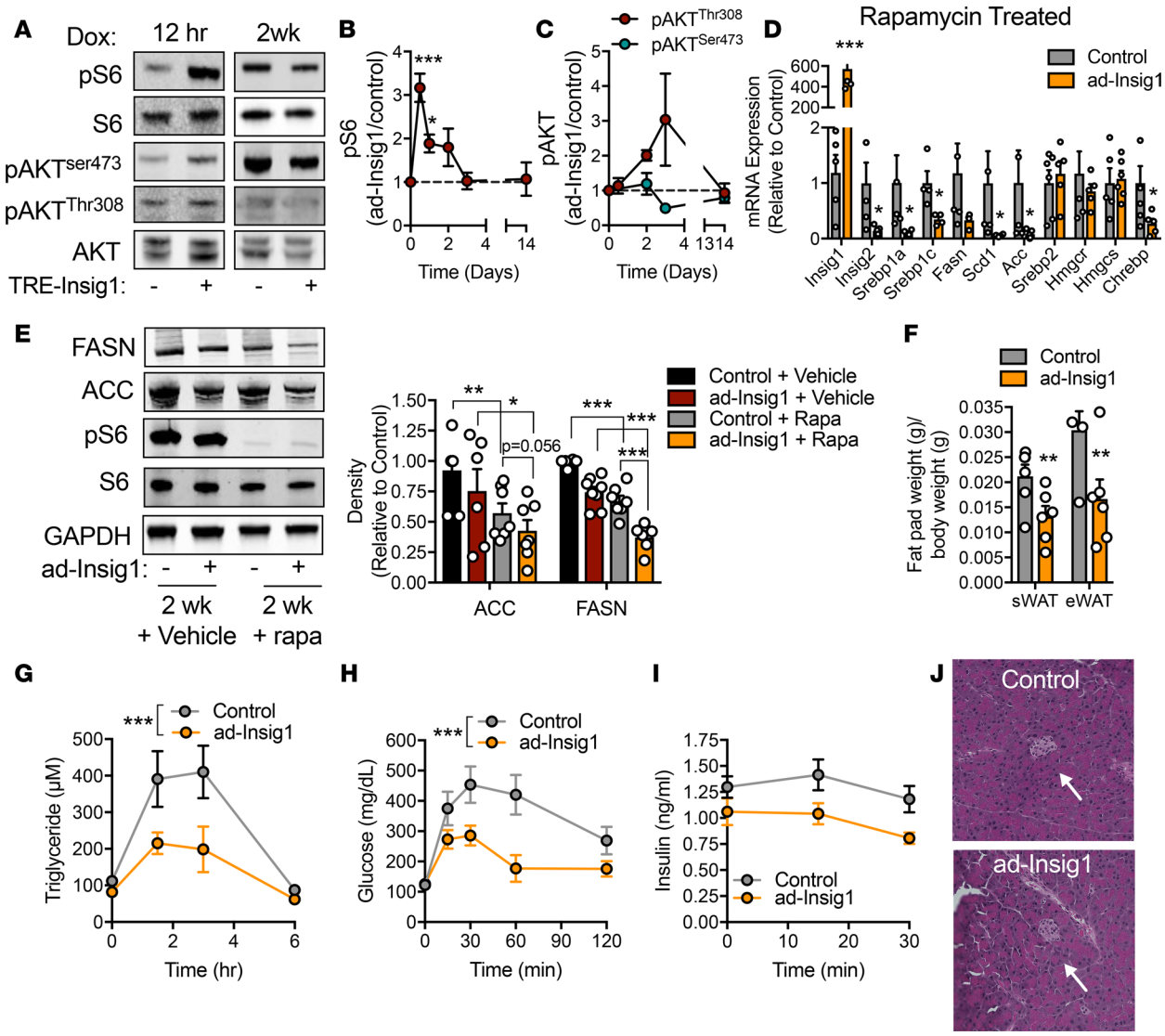

Figure 3. mTORC1 is activated in response to a block in AT lipogenesis. (**A**) Representative Western blot for the specified proteins in the sWAT of control or ad-Insig1 mice exposed to dox for 12 hours or 2 weeks. (**B** and **C**) Densitometric quantification of Western blots for (**B**) $pS6^{Ser240/244}$ or (**C**) $pAKT^{Thr308}$ and $pAKT^{ser473}$ following the indicated durations of dox exposure (n = 3–5). (**D**) Control and ad-Insig1 mice were injected with rapamycin (rapa;4 mg/kg) every second day for 2 weeks while on dox-containing chow. Lipogenic gene expression was determined in sWAT following the 2-week treatment (n = 5). (**E**) Representative Western blot and densitometry of sWAT FASN and ACC protein levels in control or ad-Insig1 mice with or without rapa (n = 5–7). (**F**) sWAT and eWAT weights after 2 weeks treatment with both dox and rapa (n = 5–6). (**G**) Triglyceride clearance test performed following 3 weeks of dox and rapa treatment (n = 6–7). (**H**) Oral glucose tolerance test conducted following 2 weeks of dox and rapa treatment (n = 6). (**I**) Insulin measurements during oral glucose tolerance (n = 6). (**J**) H&E stain of pancreatic islet (arrow). Original magnification, ×20. All data are presented as mean ± SEM. $^*P < 0.05$, $^{**}P < 0.01$, $^{***}P < 0.001$ by 2-tailed Student's t test (bar graphs) or 2-way ANOVA (systemic assays). The Tukey correction was used for multiple comparisons. In all cases, for a given condition, representative Western blot images are from the same sample, although the target proteins may have been probed on separate membranes to facilitate clear visualization. All densitometry was conducted on samples run on the same gel.

of phospho-AKT (Ser^{473} and Thr^{308}) were not altered at any time point on diet in ad-Insig1 mice (Figure 3C). To determine if mTORC1 played a causative role in lipogenic compensation, we treated control and ad-Insig1 mice with rapamycin, an inhibitor of mTORC1 activity. We validated the dosage of rapamycin by demonstrating that, at the dose chosen, rapamycin was able to suppress mTORC1 activity in AT of high-fat diet–induced obese mice, a condition in which mTORC1 activity is typically enhanced (Supplemental Figure 4A). We found that, in the absence of mTORC1 signaling by rapamycin treatment, 2 weeks of Insig1 overexpression maintained the suppression of SREBP1 and ChREBP lipogenic genes, whereas SREBP2 and downstream targets HMGCR and HMGCS were unaltered (Figure 3D). Furthermore, the 2-week rapamycin regimen resulted in decreased protein levels of FASN and ACC compared with vehicle treated

mice regardless of genotype (Figure 3E). Insig1 overexpression was synergistic with rapamycin treatment, as ad-Insig1 mice injected with rapamycin displayed greater suppression of lipogenic protein levels compared with control mice treated with rapamycin (Figure 3E). The combination of Insig1 overexpression and rapamycin treatment led to a significant reduction in white fat pad weight (Figure 3F) and marked improvements in both TG clearance (Figure 3G) and glucose tolerance (Figure 3H). The glucose and TG clearance curves in the control mice are reminiscent of a diabetic mouse, likely because rapamycin has been shown to cause β cell toxicity, resulting in peripheral insulin resistance (25). Even so, we can demonstrate that improvements in oral and TG clearance in ad-Insig1 mice are not due to differential effects of rapamycin on control and ad-Insig1 mice. Glucose-stimulated insulin secretion was not different between groups; if fact, insulin secretion in ad-Insig1 mice trended lower than in control mice (Figure 3I). Furthermore, islet size was similar between genotypes (Figure 3J). We confirmed the rapamycin results with a genetic mouse model in which we simultaneously overexpressed Insig1 and knocked out the regulatory-associated protein of mTOR (raptor), the regulatory protein required for mTORC1 activity. We did this by crossing ad-Insig1 mice with raptor-floxed mice carrying the TRE-Cre transgene (raptor aKO) to produce an adipocyte-specific, inducible model of insig1 overexpression in a raptor-KO background (Supplemental Figure 4, B and C). Overexpression of Insig1 in a raptor aKO background for 2 weeks resulted in suppression of most TG synthesis genes, but not HMGCR and HMGCS, compared with raptor aKO mice alone (Supplemental Figure 4D), a result consistent with the rapamycin treated mice (Figure 3D). Furthermore, raptor aKO mice overexpressing insig1 displayed a reduction in sWAT depot weight (Supplemental Figure 4E) and mild improvements in both glucose tolerance (Supplemental Figure 4F) and TG clearance (Supplemental Figure 4G). However, unlike the rapamycin experiment, Insig1 overexpression in raptor aKO mice resulted in significant induction of *Chrebpα* and *Chrebpβ* transcripts (Supplemental Figure 4D). Activation of ChREBP in this context likely partially masked the Insig1 effect, accounting for the difference in phenotype intensity between the rapamycin treatment and raptor-KO experiments (Figure 3 and Supplemental Figure 4). Regardless, these data suggest that mTORC1 activity is essential for the compensatory mechanism observed in ad-Insig1 mice.

Adipocytes have a high basal flux through lipogenesis, so it is plausible that a sudden blockade of this pathway may result in enhanced TCA cycle flux and mitochondrial ROS production, as carbons (citrate) that are normally siphoned off for lipogenesis are now forced into ATP production. As a result, this may initiate a mechanism to activate mTORC1, since the kinase activity of this complex can be regulated by glycolytic flux, glucose and fructose concentrations, oxidative stress, and cellular energy levels (13, 26, 27). In support of this hypothesis, the mRNA expression of the mitochondrial citrate transporter (CiC) is significantly reduced in ad-Insig1 AT 12 hours after Insig1 induction and increased in expression during the compensatory phase (3 days dox) and then returned to control levels by 2 weeks (Figure 4A). This is a similar expression pattern, as seen for other lipogenic genes (Figure 1, G and H, and Supplemental Figure 1C), which is a result consistent with previous literature that demonstrates CiC expression is under the regulation of SREBP1 (28). A predicted consequence of reduced CiC expression is a buildup of TCA cycle and glycolytic intermediates. Mice were treated with dox for 4 hours. During the last 30 minutes mice were gavaged with a 1:1 glucose/fructose solution, and sWAT was analyzed for glycolytic and TCA cycle intermediate concentrations. Under these conditions, we detected a significant increase in fructose-1-phosphate and fructose-6-phosphate in ad-Insig1 sWAT compared with controls (Figure 4B). Furthermore, both isocitrate and pyruvate concentrations were increased in ad-Insig1 sWAT compared with that of the control (Figure 4B). This metabolite profile is to be expected, as citrate is converted to isocitrate in the next step of the TCA cycle. The reaction immediately downstream of isocitrate is rate limiting (isocitrate dehydrogenase), explaining the steady-state increase in isocitrate. Furthermore, preventing citrate efflux from the mitochondria would also induce inhibition of upstream pyruvate dehydrogenase through acetyl-coA–mediated product inhibition, allowing pyruvate and fructose-1 and -6 phosphate concentrations to rise. To establish a direct connection between high glycolytic activity and mTORC1 activation in AT, we treated wild-type mice with fructose in the drinking water for 12 hours and analyzed sWAT for pS6 levels. Fructose-treated mice displayed significantly higher levels of pS6 and pAKT^{Thr308} (Figure 4C). To determine if the observed alterations in glycolytic and TCA cycle activity were associated with oxidative stress, we treated control and ad-Insig1 mice with dox for 8 hours, a time point before the compensatory mechanism was activated. We found that protein carbonylation trended toward an increase in ad-Insig1 mice, a secondary measure of oxidative stress (Figure 4D). Moreover, ad-Insig1 AT contained significantly higher antioxidant

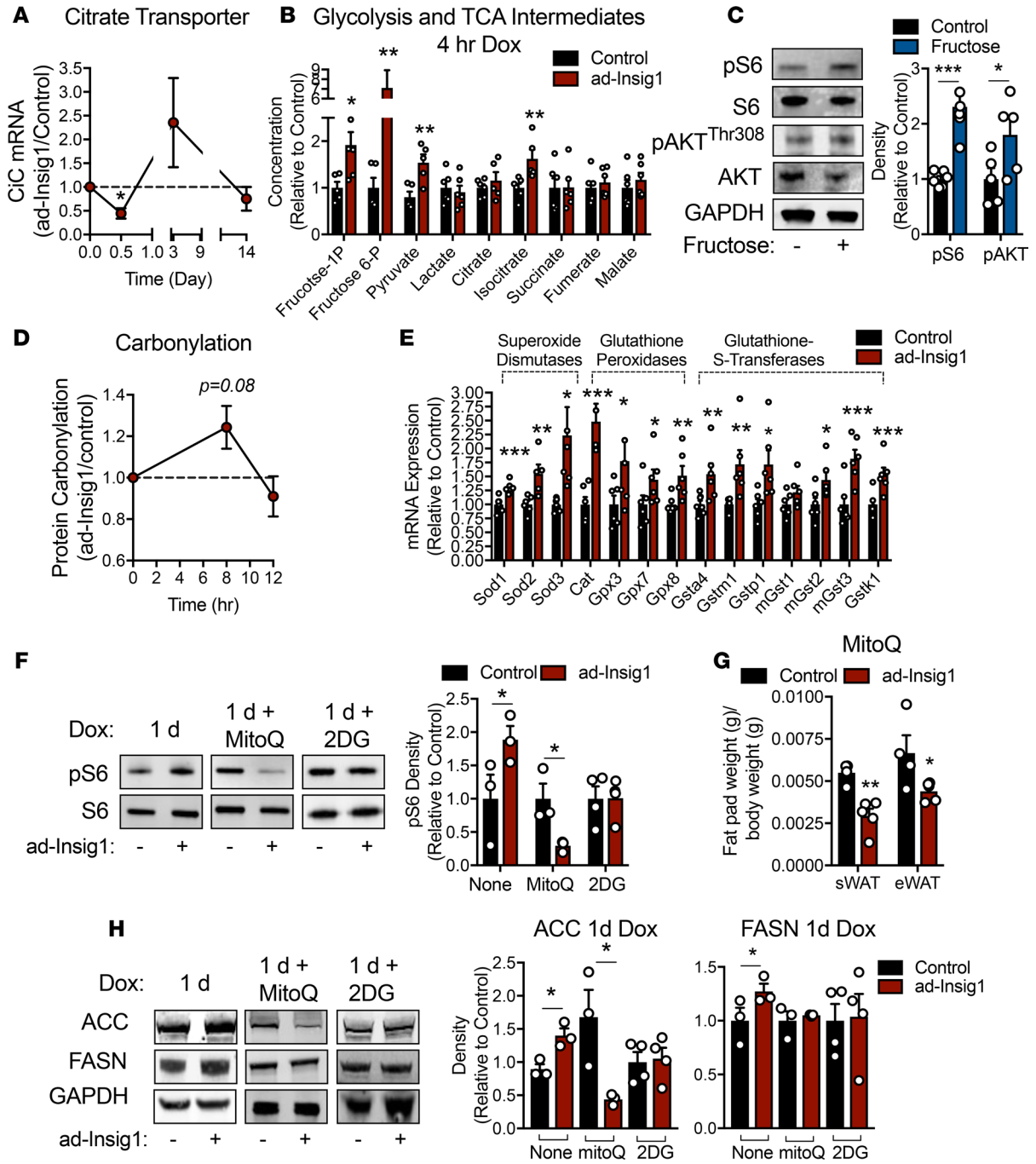

Figure 4. Acute suppression of AT DNL induces mitochondrial oxidative stress, resulting in mTORC1 activation. (**A**) mRNA expression in sWAT of the citrate transporter (CiC) over the indicated dox treatment duration (n = 8–12). (**B**) Mice were injected with dox (2 mg/kg). At 3.5 hours after injection mice were gavaged with 1:1 glucose/fructose. At 4 hours after dox injection sWAT was harvested for determination of glycolytic and TCA cycle intermediate concentrations. (**C**) Wild-type mice were treated with and without 20% fructose in the drinking water for 12 hours. A representative Western blot and densitometry for $pS6^{Ser240/244}$ and $pAKT^{Thr308}$ in sWAT (n = 5) are shown. (**D**) Protein carbonylation blot densitometry over the indicated time course of dox exposure (n = 4). (**E**) qPCR analysis of antioxidant genes in sWAT 8 hours after an injection of 2 mg/kg dox (n = 6). (**F** and **H**) Control or ad-Insig1 mice were injected with 5 mg/kg MitoQ or 250 mg/kg 2-DG and simultaneously supplied dox-supplemented diet for 24 hours. (**F**) Representative Western blot and densitometry of $pS6^{Ser240/244}$ from the sWAT of control or ad-Insig1 mice treated with or without MitoQ or 2-DG (n = 3–4). (**G**) AT depots weights with MitoQ treatment. (**H**) An example Western blot for ACC and FASN levels in sWAT from control or ad-Insig1 mice treated with MitoQ or 2-DG and corresponding densitometry (n = 3–4). In this instance FASN was run on a separate gel from ACC and GAPDH although the biological sample presented is consistent. All data are presented as mean ± SEM. $^*P < 0.05$, $^{**}P < 0.01$, $^{***}P < 0.001$ by 2-tailed Student's t test. In all cases, for a given condition, representative Western blot images are from the same sample, although the target proteins may have been probed on separate membranes to facilitate clear visualization. All densitometry was conducted on samples run on the same gel.

enzyme mRNA expression (Figure 4E), further indication of active oxidative stress. Previous studies have shown that mTORC1 can be positively or negatively regulated by ROS in a cell type– and ROS dose-dependent manner (29). To determine if mitochondrial ROS production during initial Insig1 overexpression is responsible for mTORC1 activation, we treated control and ad-Insig1 mice with mitoQ, a mitochondrially targeted antioxidant compound. During the phase of overcompensation (1-day dox exposure) sWAT from ad-Insig1 mice treated with mitoQ for 1 day displayed a significant reduction in pS6 levels compared with that of control mice under the same regimen (Figure 4F). This is in contrast to the observed increase in pS6 level at 1 day of dox feeding without mitoQ treatment (Figure 4F). MitoQ treatment resulted in significantly lower sWAT and eWAT mass (Figure 4G) and suppression of ACC protein expression in ad-Insig1 mice (Figure 4H). However, FASN levels were unaltered (Figure 4H). As further evidence for a substrate-driven mechanism of mTORC1 activation, 2-deoxy-glucose (2-DG) treatment, to reduce glycolytic flux, prevented the increase in pS6, ACC, or FASN observed following 1-day dox exposure (Figure 4, F and H). Thus, both MitoQ and 2-DG treatment are sufficient to prevent the compensatory activation of mTORC1 and the overcompensation of lipogenic enzyme expression characteristic of the 1-day time point. However, these treatments did not fully suppress the compensation, suggesting that the ROS/mTORC1 pathway is not the only route to compensation. ChREBP is a potential parallel pathway that is activated by high glycolytic intermediate concentrations and may participate in enhancing lipogenic enzyme expression at the 1-day time point (Supplemental Figure 2).

The above data suggest that substrate flux through glycolysis and the TCA cycle is required for the redox signal responsible for mTORC1-mediated compensation of the adipocyte DNL suppression. However, mTORC1 activation is resolved within 3 days of Insig1 overexpression, suggesting another mechanism takes over for chronic compensation. We found that ad-Insig1 sWAT had higher fructose transporter (GLUT5) mRNA content compared with controls at 3 days and 2 weeks after dox administration (Figure 5A), suggesting DNL substrate availability may also be important for chronic compensation. At the protein level, GLUT5 was not changed at 1 or 3 days of dox feeding but was significantly increased at 2 weeks on dox diet (Figure 5B). Protein levels of GLUT4, the insulin-sensitive glucose transporter, were unaltered in ad-Insig1 sWAT regardless of time on the dox diet (Figure 5B). These data suggest that the upregulation of GLUT5 does not participate in the initial compensatory mechanism but may be important for chronic compensation in response to DNL suppression. In keeping with this hypothesis, GLUT5 upregulation was maintained in ad-Insig1 sWAT, even during rapamycin treatment, suggesting GLUT5 expression is not regulated by mTORC1 activity (Figure 5C). Additionally, fructose treatment of WT mice moderately increased the expression of GLUT5 but did not affect the expression of GLUT4 (Figure 5D). We went on to determine if feeding ad-Insig1 mice a dox-containing ketogenic diet, which lacks DNL substrates, will prevent the compensation. Control mice fed a ketogenic diet for 3 weeks inherently displayed lower ACC and FASN gene expression compared with those on a chow diet (Supplemental Figure 5A). We observed that Insig1 overexpression during the ketogenic diet reduced sWAT fat pad mass (Figure 5E) and suppressed all TG synthesis gene expression to a greater extent than the ketogenetic diet in control mice (Figure 5F and Supplemental Figure 5). Interestingly this dietary regimen did not promote Insig1 actions on the cholesterol synthesis pathway (Figure 5F). To ensure that these results were due to the lack of lipogenic substrates, not ketosis per se, we treated mice with 2-DG in the drinking water, in addition to dox, for 2 weeks. 2-DG did not alter lipogenic gene expression in control mice (Supplemental Figure 5). However, similarly to the ketogenic diet, 2-DG feeding resulted in a reduction of fat pad mass in ad-Insig1 mice (Figure 5G). This was accompanied by a significant decrease in TG synthesis genes but not cholesterol synthetic genes in ad-Insig1 sWAT (Figure 5H). These data provide further evidence that substrate availability is essential for chronic compensation of the adipocyte to a block in SREBP1-mediated lipogenesis (Figure 6).

Discussion

ChREBP is considered to be a more robust regulator of lipogenic gene expression in adipocytes compared with SREBP1. This is primarily based on KO mouse models. Here, we reveal insights into AT DNL by perturbing the system transiently in the adult mouse and analyzing the adaptation of the adipocyte. Twelve hours after Insig1 induction, we observed a robust suppression of DNL enzyme levels in AT (Figure 1, G and I). Interestingly, this effect was immediately followed by ROS-mediated activation of mTORC1. This mechanism resulted in enhanced processing of SREBP1 (Figure 1J) and restoration of lipogenic gene expression. This cannot, however, be the only compensatory mechanism, because AT from whole-body SREBP1-null mice has normal levels of lipogenic gene mRNAs, suggesting the activation of a redundant pathway. Therefore, it is likely that

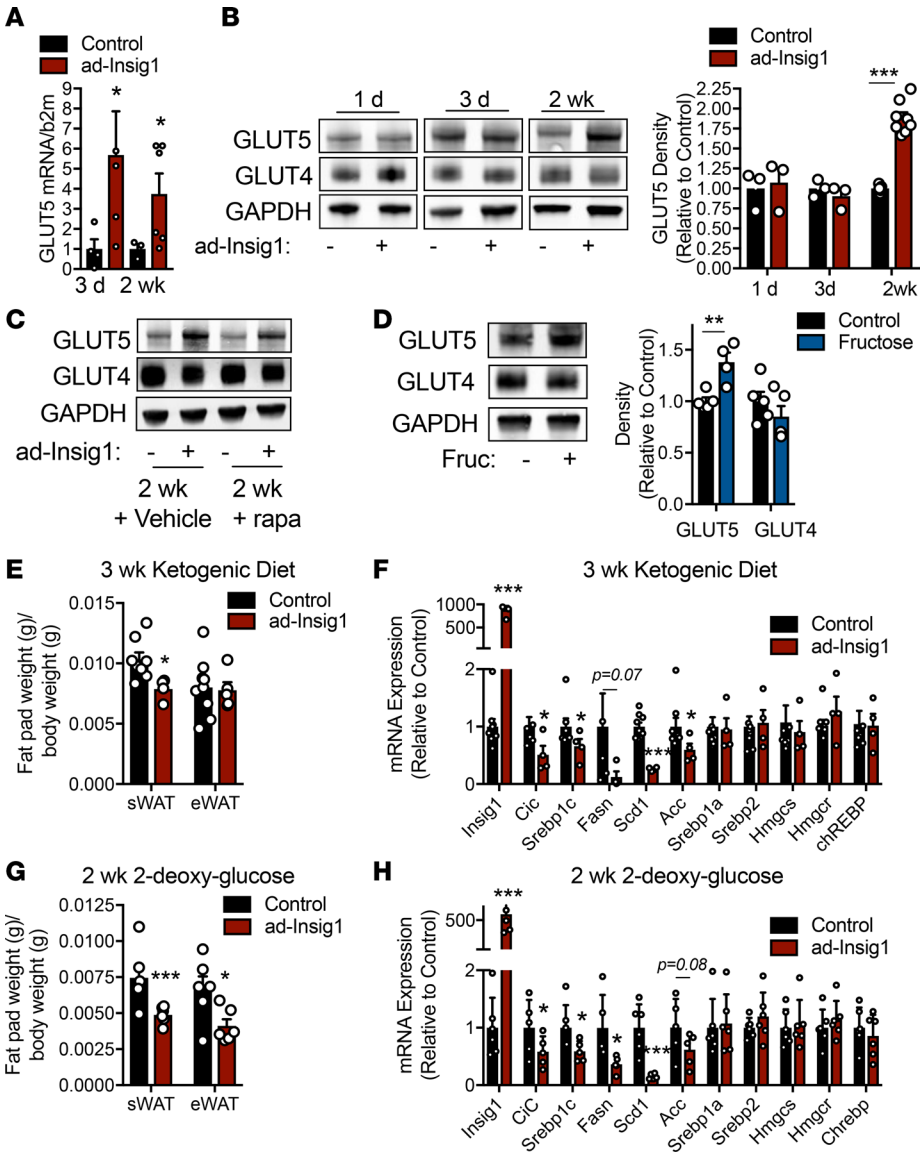

Figure 5. Chronic compensation to DNL suppression is dependent on substrate availability. (**A**) GLUT5 mRNA expression in control or ad-Insig1 mice at the indicated time points on dox diet. (**B**) Western blot image and corresponding densitometry for GLUT4 and GLUT5 in sWAT of control or ad-Insig1 mice following the indicated duration of dox treatment in the diet (n = 3–8). (**C**) Representative Western blot of n = 3 from the sWAT of control or ad-Insig1 mice following 2 weeks of dox treatment with rapamycin (rapa) or vehicle injections. (**D**) Wild-type mice were treated with or without 20% fructose in the drinking water for 12 hours. A representative Western blot and densitometry for GLUT4 and GLUT5 in sWAT (n = 5) is shown. (**E** and **F**) Control and ad-Insig1 mice were supplied with a ketogenic diet containing dox for 3 weeks, after which (**E**) sWAT and eWAT weight were measured and (**F**) DNL gene expression was quantified (n = 5–7). (**G** and **H**) Mice were provided with 2-DG in the drinking water (0.5%) in addition to the dox diet. Following 2 weeks treatment (**G**) sWAT and eWAT weights were measured and (**H**) lipogenic enzyme mRNA was quantified (n = 5–6). All data are presented as mean ± SEM. $^*P < 0.05$, $^{**}P < 0.01$, $^{***}P < 0.001$ by 2-tailed Student's t test. In all cases, for a given condition, representative Western blot images are from the same sample, although the target proteins may have been probed on separate membranes to facilitate clear visualization. All densitometry was conducted on samples run on the same gel.

ChREBP also participates in restoring lipogenesis in the context of SREBP1 pathway inhibition. Our data provide some evidence for this, as ChREBP levels trend toward an increase in ad-Insig1 mice treated with dox for 1 day (Supplemental Figure 2). However, the data are highly variable, precluding any firm conclusions. Based on mouse models with an adipocyte-specific ChREBP-KO, we know that SREBP1 does not compensate for ChREBP activity, as suppression of lipogenic genes in AT is maintained (15). We suggest this observation cannot serve as evidence for a greater importance of ChREBP in AT DNL regulation. Rather, it reflects the

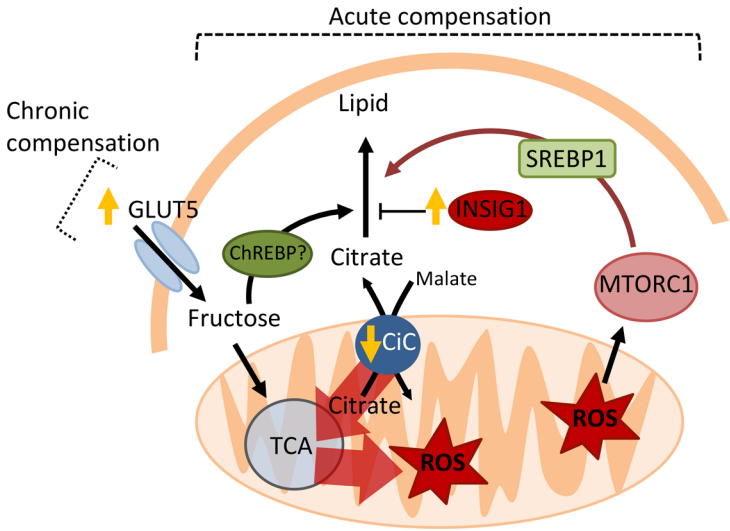

Figure 6. Model for mTORC1-mediated compensation of obstructed AT lipogenesis. Insig1 overexpression results in general suppression of lipogenic gene expression, including that of the citrate transporter (CiC). Diminished efflux of citrate from the mitochondria results in a "backup" of the TCA cycle and mitochondrial ROS production, as citrate carbons are abruptly diverted into the TCA cycle for ATP production instead of lipogenesis. ROS activates mTORC1, which stimulates both SREBP1 transcription and the processing of SREBP1 into its nuclear/active from. High levels of glycolytic intermediates may also stimulate ChREBP activity. The consequence is restoration of lipogenic gene expression. This mechanism of compensation is transient, but chronic compensation is maintained by greater uptake of fructose via GLUT5. Both acute and chronic compensation is dependent on DNL substrate availability.

dual role of ChREBP in regulating both DNL and glycolysis (14, 15). In this study, we have found that the redox regulation of the mTORC1/SREBP1 pathway is dependent on DNL substrate availability, as fructose feeding enhances adipocyte pS6 levels and 2-DG treatment prevents the initial increase in pS6 observed after dox induction of Insig1. Therefore, we predict that the strong suppression of AT lipogenesis in ChREBP-KO mice and the inability of SREBP1 to compensate is by virtue of the additional blockade of glycolysis. In fact, if we mimic inhibition of glycolysis by feeding ad-Insig1 mice with a ketogenic diet, devoid of glycolytic substrates, or 2-DG we could maintain suppression of lipogenic gene expression to a similar level as ChREBP-null mice (15). Therefore, the relationship between ChREBP and SREBP1 is likely complementary in AT, as has been described in the liver.

We found that the initiating mechanism of compensation after Insig1 overexpression involves ROS-mediated activation of mTORC1. ROS can stimulate mTORC1 activity through oxidation of cysteine residues in the complex (29). This may explain why mTORC1 activation in our model is independent of AKT activity (Figure 3C). Interestingly, this mechanism is likely specific to the adipocyte, as constitutive models of liver DNL blockade, such as Insig1 overexpression or whole-body SCAP KO, do not show signs of a cell-autonomous mechanism for compensation (19, 30). Interestingly, mice fed fructose display a *reduction* in liver pS6 levels (27), the opposite of our finding reported here in adipocytes. It is likely that inherent differences between hepatocytes and adipocytes give way to divergent regulation of mTORC1 activity, such as differences in basal antioxidant capacity. Consequently, hepatocytes do not activate mTORC1 to compensate for obstructed lipogenesis. It is also likely that both cell types differentially regulate mTORC1 in a ROS concentration-dependent manner, as previous studies have shown that low concentrations of ROS stimulate mTORC1 activity, whereas high doses suppress activity in various cell lines (31). In fact, a mouse model of adipocyte-specific glutathione depletion, which results in oxidative stress, displays a reduction in SREBP1-regulated DNL mRNA expression (32). Although mTORC1 activity was not measured in this study, the changes in SREBP1 transcriptional activity could be explained by mTORC1 inhibition via high ROS doses, an effect opposite from what would be expected at doses within the lower physiological range. Thus, differences in the response of liver and AT to suppression of lipogenesis likely have a multifactorial explanation involving lipogenic substrate flux, ROS generation rates, and basal antioxidant capacity. This may also be true for the response between different adipose depots, as BAT did not compensate for Insig1 overexpression at 3 days of dox treatment (Supplemental Figure 1C).

The transient changes in AT lipogenic capacity produced in ad-Insig1 mice result in changes in whole-body glucose and TG metabolism (Figure 2). The prevailing claim is that whole-body insulin sensitivity positively correlates with AT DNL (8, 33–35). Functionally, this is true for ChREBP-mediated DNL, as mice overexpressing ChREBP in the adipocyte display lower body weight on a Western diet, improved insulin sensitivity, reduced hepatic TG content, and a beige adipocyte gene expression profile (36). Conversely, adipocyte-specific ChREBP-KO mice are insulin resistant (15). Consistent with these results, we report here that Insig1-mediated suppression of AT DNL results in slight glucose intolerance before compensation is fully initiated (Figure 2A). However, when contemplating the question of whether we should be therapeutically activating or inhibiting AT DNL to improve metabolic homeostasis in disease states, we need to consider all effects of AT DNL on physiology. The most striking phenotypic change we observed is an improvement in TG clearance with Insig1 overexpression before compensation or under conditions that prevent compensation (Figure 2B, Figure 3G, and Supplemental Figure 4G). These data suggest that AT SREBP1-regulated DNL may negatively regulate whole-body lipid clearance. In keeping with this, previous studies have shown that a KO of FASN in adipocytes displays a beneficial effect on whole-body metabolism: improved glucose tolerance, increased energy expenditure, adipocyte beiging, and resistance to diet-induced obesity (37). In contrast, activating adipocyte DNL by overexpressing the nuclear form of SREBP1a using an aP2 promoter increases the release of fatty acids, resulting in hepatic steatosis (38). A further consideration for the role of AT DNL in metabolic syndrome is its involvement in adipogenesis, as production of new adipocytes in obesity is one hallmark of healthy AT expansion (39). FASN is required for adipogenesis, and overexpression nuclear SREBP1c inhibits adipocyte differentiation, causing lipodystrophic and diabetic phenotype (37, 40). Therefore, further work is required to determine if enhancing or suppressing AT lipogenesis is a viable approach to treat metabolic conditions, such as type 2 diabetes. The answer is likely dependent on the pathway of DNL that is to be manipulated. Although both ChREBP and SREBP1 pathways regulate DNL gene expression in AT, as explained above, they do diverge in their metabolic function at both the cellular and organismal levels. Particularly important are potential differences in the specific bioactive lipid species produced by each pathway and how each pathway regulates adipogenesis.

Our study makes evident the use of inducible genetic systems to establish the importance of a pathway in cellular homeostasis in vivo. Identifying mechanisms of compensation following a perturbation in the adult animal can be a highly valuable endeavor to determine if a pharmacological intervention will have sustained efficacy in the targeted tissue. For example, treatment of mice with neuropeptide Y (NPY) has been shown reduce food intake and promote weight loss in rodents; however, whole-body KO of this peptide in mice does not affect body weight regulation. By using a dox-inducible NPY-KO mouse, Ste Marie et al. demonstrated that NPY depletion does not alter feeding habits although did transiently effect body weight (41). The conclusion of this study was that, due to the likely compensation that occurs in response to NPY deletion, NPY targeting therapy may not have sustainable benefit on food intake. Here, we used a similar approach, inducibly overexpressing Insig1 in adipocytes of adult mice to mimic the sterol-induced sequestration of SREBPs by the Insig1/SCAP complex. We have demonstrated that mTORC1 is essential for the maintenance of adipocyte lipogenesis when DNL substrates are available. Through this mechanism and ChREBP activity, the adipocyte can maintain lipogenesis even under conditions that would inhibit lipogenesis in other cell types to guarantee adequate storage of otherwise toxic carbohydrates.

Methods

Animals. Insig1 was inducibly overexpressed in mature adipocytes using a TRE-driven Insig1 construct. The mouse *Insig1* gene was subcloned into the pTRE vector (Clontech Laboratories, 631059) with a rabbit β-globin 3′ UTR. Specificity for the adipocyte in this model was accomplished by using the rtTA under the control of the adiponectin promoter (42). Mice expressing both the TRE-Insig1 and rtTA transgenes did not express Insig1 until dox was present (Figure 1B). Raptor-floxed mice were purchased from The Jackson Laboratory (B6.Cg-Rptor$^{tm1.1Dmsa}$/J; no. 013188). All cohorts of mice were male and 10–15 weeks old.

Mouse treatments. Insig1 gene expression was induced with mouse chow, high-fat diet, or ketogenic diet containing 600 mg/kg dox (Bio Serve, S4107, S7597, S5867). MitoQ (a gift from Mike Murphy, University of Cambridge, Cambridge, United Kingdom) was dissolved in PBS, 5% DMSO. Mice were injected i.p. with a single 5 mg/kg injection of MitoQ at the initiation of dox chow feeding. Rapamycin (LC Laboratories, R-5000) was dissolved in 100% ethanol at a concentration of 50 mg/kg. Aliquots were made and stored at –80°C. The day of injections a 1 mg/ml rapamycin stock was prepared in a solution containing

10% PEG400, 10% tween80, and ddH_2O. Mice were injected with 4 mg/kg every second day. Where indicated, mice received a single 250 mg/kg 2-DG (MilliporeSigma, D6134) injection at the initiation of dox chow feeding. 2-DG was dissolved in PBS. When 2-DG was supplied in the drinking water it was dissolved in ddH_2O to 0.5% (w/v) and filter sterilized. Fructose was dissolved to 20% (w/v) in ddH_2O, filter sterilized, and supplied as drinking water for the 12-hour fructose treatment studies.

Metabolic phenotyping. For the oral glucose tolerance test, mice were fasted for 3 hours before to the administration of glucose (1.25 g/kg body weight) by gastric gavage. At the indicated time points, venous blood samples were collected in capillary tubes from the tail veins. Glucose levels were measured using an oxidase-peroxidase assay. Insulin concentration was determined using a commercial Insulin Elisa Kit (Crystal Chem, 90095). For the TG clearance procedure, mice were fasted for 15 hours and then gavaged with 20% Intra-lipid (15 μL/g body-weight; MilliporeSigma, I141).

Western blot. Protein was extracted from AT by homogenization in PBS supplemented with 1 mM EDTA, 20 mM NaF, 2 mM Na_3VO_4, and protease inhibitor cocktail. 5× RIPA buffer was added to the homogenate for a final concentration of 10 mM Tris-HCl, 2 mM EDTA, 0.3% NP40, 0.3% deoxycholate, 0.1% SDS, and 140 mM NaCl, pH 7.4. The sample was cleared by centrifugation at 10,000 *g* for 5 minutes. 20–50 μg/lane of supernatant protein was separated by SDS-PAGE (Thermo Fisher, NP0335BOX) and transferred to nitrocellulose membrane. The blots were then incubated overnight at 4°C with primary antibodies in a 1% BSA TBST-blocking solution. The Odyssey Infrared Imager was used to visualized Western blots with Li-Cor IRdye secondary antibodies. Please see Supplemental Table 2 for a list of all primary and secondary antibodies, including sources. See complete unedited blots in the supplemental material.

qPCR. Tissues were homogenized in TRIzol (Fisher Scientific, 12034977) using the Qiagen TissueLyser II. RNA was isolated per the manufacturer's protocol. RNA quality and yield were determined by absorbance at 260 nm, 280 nm, and 230 nm. cDNA was prepared by reverse transcribing 1 μg RNA with the iScript cDNA Synthesis Kit (Bio-Rad, 1708890). The results were calculated by the standard threshold cycle method and were used for normalization. Please refer to Supplemental Table 1 for qPCR primer sequences.

Nuclear and ER membrane fractionation. Freshly harvested sWAT was homogenized with a motor-driven Teflon/glass homogenizer in 10 ml ice cold buffer (10 mM MOPS, 1 mM EDTA, 210 mM mannitol, 70 mM sucrose, 20 mM NaF, 2 mM Na_3VO_4, and protease inhibitor cocktail, pH 7.4). The nucleus was pelleted by centrifugation at 720 *g* for 10 minutes. The pellet was resuspended in 10 ml of the same buffer and filtered through cheesecloth. The cleared sample was centrifuged again at 720 *g* for 10 minutes. The nuclear pellet was resuspended in PBS. The supernatant from the first 720 *g* spin was centrifuged at 30,000 *g* to recover ER-enriched cellular membranes. The ER pellet was resuspended in PBS. Following protein determination, fractions were subjected to Western blot analysis for processed SREBP1 (nuclear fraction) and precursor SREBP1 (membrane fraction).

Histology. sWAT was excised and fixed in 10% PBS-buffered formalin for 24 hours. Tissues were paraffin embedded and sectioned (5 μm) at the University of Texas Southwestern Molecular Pathology Core. Following hydration, tissues were stained with H&E.

Ex vivo lipolysis assay. sWAT was harvested and washed in cold PBS. Small pieces of AT (~50 mg) were equilibrated for 1 hour in 150 μL DMEM containing 2% BSA. AT pieces were then transferred into another culture dish containing 200 μL lipolysis buffer (5 mM HEPES, 125 mM NaCl, 5 mM KCl, 1.8 mM $CaCl_2$, and 2.6 mM $MgSO_4$, pH 7.4) in the presence or absence of isoproterenol (10 μm; MilliporeSigma, I6504). Explants were incubated for 2 hours at 37°C. Buffer was removed from the explants and assayed for glycerol using the Free Glycerol Determination Kit (MilliporeSigma, F6428). Final glycerol values were normalized to total weight (grams) of tissue in the corresponding well.

LC/MS/MS analysis of hexose phosphate TCA cycle intermediates. Clamp-frozen tissue sections (100 mg) were homogenized with a mechanical tissue disruptor in 0.8 mL of 80% methanol in a screw cap borosilicate glass tube. The homogenizer probe was rinsed with 1.6 mL of 80% MeOH, and the methanolic solution was combined with the homogenate. The tissues were kept on ice during the homogenization/quenching process. Immediately afterward 40 μL of internal solution was added [7-methyluric acid (2,4,5,6-$^{13}C_4$, 99%, 1,3,9-$^{15}N_3$, 98%) 25 μg/mL] (Cambridge Isotope Laboratories Inc.). Samples were thoroughly vortexed and then centrifuged in a benchtop centrifuge at 2,500 *g* (Sorvall Legend XTR, Thermo Fisher Scientific). Supernatant was transferred to a 5.0-mL polypropylene cell culture tube. Protein pellets were reextracted with 2 mL of 80% MeOH, and the supernatants were combined. Tissue extracts were dried in a speed-vap concentrator (CentriVap Concentrator, Labconco). The dried residues were reconstituted in 220 μL of H_2O 0.1% formic acid for TCA cycle intermediates and H_2O 10 mM tributyl amine for hexose phosphates. Reconstituted samples were transferred to GC vials.

TCA intermediates were analyzed by injecting 1 μL of sample into the LC/MS/MS system consisting of a Shimadzu LCMS-8060 triple quadrupole mass spectrometer operating the DUIS ion source in electrospray mode (Shimadzu Scientific Instruments) coupled to a Nexera X2 UHPLC chromatographer equipped with 3 pumps, autosampler SIL-30AC, and CTO-20AC (Shimadzu Scientific Instruments). Compounds were resolved and analyzed using the instrumental parameters and chromatographic conditions described in the Shimadzu LC/MS/MS method package for cell culture profiling (Shimadzu Scientific Instruments). Hexose phosphate intermediates were analyzed by injecting 5 μL of sample in the same LC/MS/MS system. Compound was resolved by combining ion pair chromatography and differential fragmentation patterns (43, 44). Data were processed using the LabSolutions V 5.82 and LabSolutions Insight V 2.0 program packages (Shimadzu Scientific Instruments).

Statistics. All data are presented as mean ± SEM. Statistical analyses were performed with 2-tailed Student's *t* test or, in the case of systemic assays, 2-way ANOVA. A *P* value of less than 0.05 was determined to be statistically significant. All qPCR data points were the average of technical duplicates. For all mouse studies, the *n* value corresponds to individual mice of a given treatment. Data were analyzed used Prism GraphPad software.

Study approval. All animal experimental protocols were approved by the Institutional Animal Care and Use Committee of the University of Texas Southwestern Medical Center.

Author contributions

CC conceptualized the project, designed experiments, analyzed and interpreted data, conducted experiments, with the exception of those listed below, and wrote the manuscript. YZ produced and validated the TRE-Insig1 mice as well as conducted chronic high-fat diet studies. VAP, NJ, and ALG assisted in mouse studies and sample processing. RG conducted the LC/MS/MS analysis of TCA cycle intermediates. DYO, GL, and JDH provided guidance and were consulted for data interpretation. PES was involved in experimental design and the writing of the manuscript.

Acknowledgments

We thank the University of Texas Southwestern Transgenic Core for their help in the generation of mice. We also thank the University of Texas Southwestern Molecular Pathology Core for imbedding and sectioning samples for histology. The MitoQ compound was a gift from Mike Murphy. This study was supported by US NIH grants R01-DK55758, P01-DK088761, R01-DK099110, and P01-AG051459 as well as by an unrestricted grant from the Novo Nordisk Research Foundation (PES). The contributions of GL and JDH were supported by the NIH (HL-20948). CC is supported by NIH grant F32-DK113704. The contribution of DYO was supported by the NIH (R01-DK108773) and the American Heart Association (14SDG19880020). VAP is supported by American Diabetes Association (ADA 1-18-PMF-030). YZ is supported by NIH grant K99-DK114498.

Address correspondence to: Philipp E. Scherer, 5323 Harry Hines Boulevard, L5206; MC:8549, Dallas, Texas 75390, USA. Phone: 214.648.8715; Email: philipp.scherer@utsouthwestern.edu.

1. Kawahito S, Kitahata H, Oshita S. Problems associated with glucose toxicity: role of hyperglycemia-induced oxidative stress. *World J Gastroenterol*. 2009;15(33):4137–4142.
2. Duarte JA, et al. A high-fat diet suppresses de novo lipogenesis and desaturation but not elongation and triglyceride synthesis in mice. *J Lipid Res*. 2014;55(12):2541–2553.
3. Diraison F, Dusserre E, Vidal H, Sothier M, Beylot M. Increased hepatic lipogenesis but decreased expression of lipogenic gene in adipose tissue in human obesity. *Am J Physiol Endocrinol Metab*. 2002;282(1):E46–E51.
4. Ortega FJ, et al. The gene expression of the main lipogenic enzymes is downregulated in visceral adipose tissue of obese subjects. *Obesity (Silver Spring)*. 2010;18(1):13–20.
5. Kursawe R, et al. Decreased transcription of ChREBP-α/β isoforms in abdominal subcutaneous adipose tissue of obese adolescents with prediabetes or early type 2 diabetes: associations with insulin resistance and hyperglycemia. *Diabetes*. 2013;62(3):837–844.
6. Tang Y, et al. Adipose tissue mTORC2 regulates ChREBP-driven de novo lipogenesis and hepatic glucose metabolism. *Nat Commun*. 2016;7:11365.
7. Eissing L, et al. De novo lipogenesis in human fat and liver is linked to ChREBP-β and metabolic health. *Nat Commun*. 2013;4:1528.
8. Herman MA, et al. A novel ChREBP isoform in adipose tissue regulates systemic glucose metabolism. Nature. 2012;484(7394):333–338.
9. Horton JD, Goldstein JL, Brown MS. SREBPs: activators of the complete program of cholesterol and fatty acid synthesis in the liver. *J Clin Invest*. 2002;109(9):1125–1131.

10. Iizuka K, Bruick RK, Liang G, Horton JD, Uyeda K. Deficiency of carbohydrate response element-binding protein (ChREBP) reduces lipogenesis as well as glycolysis. *Proc Natl Acad Sci USA*. 2004;101(19):7281–7286.
11. Repa JJ, et al. Regulation of mouse sterol regulatory element-binding protein-1c gene (SREBP-1c) by oxysterol receptors, LXRalpha and LXRbeta. *Genes Dev*. 2000;14(22):2819–2830.
12. Tian J, Goldstein JL, Brown MS. Insulin induction of SREBP-1c in rodent liver requires LXRα-C/EBPβ complex. *Proc Natl Acad Sci USA*. 2016;113(29):8182–8187.
13. Caron A, Richard D, Laplante M. The roles of mTOR complexes in lipid metabolism. *Annu Rev Nutr*. 2015;35:321–348.
14. Linden AG, et al. Interplay between ChREBP and SREBP-1c coordinates postprandial glycolysis and lipogenesis in livers of mice. *J Lipid Res*. 2018;59(3):475–487.
15. Vijayakumar A, et al. Absence of carbohydrate response element binding protein in adipocytes causes systemic insulin resistance and impairs glucose transport. *Cell Rep*. 2017;21(4):1021–1035.
16. Shimano H, et al. Elevated levels of SREBP-2 and cholesterol synthesis in livers of mice homozygous for a targeted disruption of the SREBP-1 gene. *J Clin Invest*. 1997;100(8):2115–2124.
17. Sekiya M, et al. SREBP-1-independent regulation of lipogenic gene expression in adipocytes. *J Lipid Res*. 2007;48(7):1581–1591.
18. Yang T, et al. Crucial step in cholesterol homeostasis: sterols promote binding of SCAP to INSIG-1, a membrane protein that facilitates retention of SREBPs in ER. *Cell*. 2002;110(4):489–500.
19. Engelking LJ, et al. Overexpression of Insig-1 in the livers of transgenic mice inhibits SREBP processing and reduces insulin-stimulated lipogenesis. *J Clin Invest*. 2004;113(8):1168–1175.
20. Kuriyama H, Liang G, Engelking LJ, Horton JD, Goldstein JL, Brown MS. Compensatory increase in fatty acid synthesis in adipose tissue of mice with conditional deficiency of SCAP in liver. Cell Metab. 2005;1(1):41–51.
21. Porstmann T, et al. SREBP activity is regulated by mTORC1 and contributes to Akt-dependent cell growth. *Cell Metab*. 2008;8(3):224–236.
22. Owen JL, et al. Insulin stimulation of SREBP-1c processing in transgenic rat hepatocytes requires p70 S6-kinase. *Proc Natl Acad Sci U S A*. 2012;109(40):16184–16189.
23. Laplante M, Sabatini DM. An emerging role of mTOR in lipid biosynthesis. *Curr Biol*. 2009;19(22):R1046–R1052.
24. Tian J, et al. BHLHE40, a third transcription factor required for insulin induction of SREBP-1c mRNA in rodent liver. *Elife*. 2018;7:e36826.
25. Barlow AD, Nicholson ML, Herbert TP. Evidence for rapamycin toxicity in pancreatic β-cells and a review of the underlying molecular mechanisms. *Diabetes*. 2013;62(8):2674–2682.
26. Lee MN, et al. Glycolytic flux signals to mTOR through glyceraldehyde-3-phosphate dehydrogenase-mediated regulation of Rheb. *Mol Cell Biol*. 2009;29(14):3991–4001.
27. Hu Y, et al. Fructose and glucose can regulate mammalian target of rapamycin complex 1 and lipogenic gene expression via distinct pathways. *J Biol Chem*. 2018;293(6):2006–2014.
28. Infantino V, Iacobazzi V, De Santis F, Mastrapasqua M, Palmieri F. Transcription of the mitochondrial citrate carrier gene: role of SREBP-1, upregulation by insulin and downregulation by PUFA. *Biochem Biophys Res Commun*. 2007;356(1):249–254.
29. Groenewoud MJ, Zwartkruis FJ. Rheb and mammalian target of rapamycin in mitochondrial homoeostasis. *Open Biol*. 2013;3(12):130185.
30. Matsuda M, et al. SREBP cleavage-activating protein (SCAP) is required for increased lipid synthesis in liver induced by cholesterol deprivation and insulin elevation. *Genes Dev*. 2001;15(10):1206–1216.
31. Li M, et al. Multi-mechanisms are involved in reactive oxygen species regulation of mTORC1 signaling. *Cell Signal*. 2010;22(10):1469–1476.
32. Okuno Y, et al. Oxidative stress inhibits healthy adipose expansion through suppression of SREBF1-mediated lipogenic pathway. *Diabetes*. 2018;67(6):1113–1127.
33. Hoffstedt J, Forster D, Lofgren P. Impaired subcutaneous adipocyte lipogenesis is associated with systemic insulin resistance and increased apolipoprotein B/AI ratio in men and women. *J Intern Med*. 2007;262(1):131–139.
34. Ranganathan G, et al. The lipogenic enzymes DGAT1, FAS, and LPL in adipose tissue: effects of obesity, insulin resistance, and TZD treatment. *J Lipid Res*. 2006;47(11):2444–2450.
35. Song Z, Xiaoli AM, Yang F. Regulation and metabolic significance of de novo lipogenesis in adipose tissues. *Nutrients*. 2018;10.
36. Nuotio-Antar AM, et al. FABP4-Cre mediated expression of constitutively active ChREBP protects against obesity, fatty liver, and insulin resistance. *Endocrinology*. 2015;156(11):4020–4032.
37. Lodhi IJ, et al. Inhibiting adipose tissue lipogenesis reprograms thermogenesis and PPARγ activation to decrease diet-induced obesity. *Cell Metab*. 2012;16(2):189–201.
38. Horton JD, Shimomura I, Ikemoto S, Bashmakov Y, Hammer RE. Overexpression of sterol regulatory element-binding protein-1a in mouse adipose tissue produces adipocyte hypertrophy, increased fatty acid secretion, and fatty liver. *J Biol Chem*. 2003;278(38):36652–36660.
39. Hepler C, Gupta RK. The expanding problem of adipose depot remodeling and postnatal adipocyte progenitor recruitment. *Mol Cell Endocrinol*. 2017;445:95–108.
40. Shimomura I, et al. Insulin resistance and diabetes mellitus in transgenic mice expressing nuclear SREBP-1c in adipose tissue: model for congenital generalized lipodystrophy. *Genes Dev*. 1998;12(20):3182–3194.
41. Ste Marie L, Luquet S, Cole TB, Palmiter RD. Modulation of neuropeptide Y expression in adult mice does not affect feeding. *Proc Natl Acad Sci USA*. 2005;102(51):18632–18637.
42. Wang ZV, Deng Y, Wang QA, Sun K, Scherer PE. Identification and characterization of a promoter cassette conferring adipocyte-specific gene expression. *Endocrinology*. 2010;151(6):2933–2939.
43. Li Y, Ptolemy AS, Harmonay L, Kellogg M, Berry GT. Quantification of galactose-1-phosphate uridyltransferase enzyme activity by liquid chromatography-tandem mass spectrometry. *Clin Chem*. 2010;56(5):772–780.
44. Jensen UG, Brandt NJ, Christensen E, Skovby F, Norgaard-Pedersen B, Simonsen H. Neonatal screening for galactosemia by quantitative analysis of hexose monophosphates using tandem mass spectrometry: a retrospective study. *Clin Chem*. 2001;47(8):1364–1372.